

The Monoanionic π -Radical Redox State of α -Iminoketones in Bis(ligand)metal Complexes of Nickel and Cobalt

Connie C. Lu, Eckhard Bill, Thomas Weyhermüller, Eberhard Bothe, and Karl Wieghardt*

Max-Planck-Institut für Bioanorganische Chemie, Stiftstrasse 34-36, D-45470 Mülheim an der Ruhr, Germany

Received April 27, 2007

The electronic structures of nickel and cobalt centers coordinated by two α -iminoketone ligands have been elucidated using density functional theory calculations and a host of physical methods such as X-ray crystallography, cyclic voltammetry, UV–vis spectroscopy, electron paramagnetic resonance spectroscopy, and magnetic susceptibility measurements. In principle, α -iminoketone ligands can exist in three oxidation levels: the closed-shell neutral form (L^0), the closed-shell dianion ($L^{\text{red}2-}$), and the open-shell monoanion ($L^{\cdot-}$). Herein, the monoanionic π -radical form ($L^{\cdot-}$) of α -iminoketones is characterized in the compounds $[(L^{\cdot-})_2Ni]$ (**1**) and $[(L^{\cdot-})_2Co]$ (**3**), where ($L^{\cdot-}$) is the one-electron-reduced form of the neutral ligand $(t\text{-Bu})N=CH-C(\text{Ph})=O$. The metal centers in **1** and **3** are divalent, high-spin, and coupled antiferromagnetically to two ligand π radicals. These bis(ligand)metal complexes can be chemically oxidized by two electrons to give the dications $[trans-(L)_2Ni(\text{CH}_3\text{CN})_2](\text{PF}_6)_2$ (**2**) and $[trans-(L)_2Co(\text{CH}_3\text{CN})_2](\text{PF}_6)_2$ (**4**), wherein the ligands are in the neutral form.

I. Introduction

The coordination chemistry of α -iminoketone ligands is quite undeveloped relative to their α -diimine congeners.^{1–5} One possible reason for this lack is that α -iminoketones, in general, are weaker donors.⁶ A search through the Cambridge Structural Database for transition-metal complexes featuring bidentate α -iminoketone ligands⁷ and their reduced equivalents (generally abbreviated as $(N^{\wedge}-O^{\wedge})$) revealed a mere total of seven structures.^{2,3,8–11} Interestingly, only three of

these complexes were derived from direct metalations of an intact α -iminoketone.^{2,3} In the remaining four structures, the α -iminoketone ligand was assembled at the metal center from smaller components such as CO and isocyanide.^{8–11}

Histograms of the bond distances in the ligand backbone (Figure 1) show that these structures fall into two distinct groups.^{12,13} One group, consisting of $[(N^{\wedge}-O^{\wedge})Pd(\eta^2\text{-1-methoxycycloocten-5-yl})](\text{BF}_4)$,³ $[(N^{\wedge}-O^{\wedge})Pd(\eta^2\text{-1-methoxycycloocten-6-yl})](\text{BF}_4)$,³ and $[(N^{\wedge}-O^{\wedge})_2MnCl_2]$,¹¹ lies at the left side of the stacked histograms. Collectively, they are mid-to-late transition metals coordinated to neutral α -iminoketones with a single C–C bond and double C=N/C=O bonds.¹⁴ The second group, comprising $[(N^{\wedge}-O^{\wedge})Ti(\text{OAr})_2]$,⁹ $[(N^{\wedge}-O^{\wedge})Zr(\text{OAr})_2]$,¹⁰ and $[(N^{\wedge}-O^{\wedge})Hf(\text{diamido-}N\text{-heterocyclic-carbene})]$,⁸ lies at the right side of the histograms. They can generally be described as early transition metals coor-

* To whom correspondence should be addressed. E-mail: wieghardt@mpi-muelheim.mpg.de.

- (1) van der Poel, H.; van Koten, G. *Synth. Commun.* **1978**, *8*, 303.
- (2) Siebenlist, R.; Frühauf, H. W.; Vrieze, K.; Smeets, W. J. J.; Spek, A. L. *Eur. J. Inorg. Chem.* **2000**, 907.
- (3) Binotti, B.; Carfagna, C.; Foresti, E.; Macchioni, A.; Sabatino, P.; Zuccaccia, C.; Zuccaccia, D. *J. Organomet. Chem.* **2004**, *689*, 647.
- (4) van Vliet, M. R. P.; van Koten, G.; Rotteveel, M. A.; Schrap, M.; Vrieze, K.; Kojic-Prodic, B.; Spek, A. L.; Duisenberg, A. J. M. *Organometallics* **1986**, *5*, 1389.
- (5) van Vliet, M. R. P.; van Koten, G.; van Beek, J. A. M.; Vreize, K.; Muller, F.; Stam, C. H. *Inorg. Chim. Acta* **1986**, *112*, 77.
- (6) Friedel, H.; Renk, I. W.; tom Dieck, H. *J. Organomet. Chem.* **1971**, *26*, 247.
- (7) Related ligands such as α -ketopyridines and *o*-aminophenolates were excluded from this search.
- (8) Spencer, L. P.; Fryzuk, M. D. *J. Organomet. Chem.* **2005**, *690*, 5788.
- (9) Chamberlain, L. R.; Durfee, L. D.; Fanwick, P. E.; Kobriger, L. M.; Latesky, S. L.; McMullen, A. K.; Steffey, B. D.; Rothwell, I. P.; Folting, K.; Huffman, J. C. *J. Am. Chem. Soc.* **1987**, *109*, 6068.
- (10) McMullen, A. K.; Rothwell, I. P.; Huffman, J. C. *J. Am. Chem. Soc.* **1985**, *107*, 1072.

(11) Szevéryni, Z.; Fülöp, V.; Kálmán, A.; Simándi, L. I. *Inorg. Chim. Acta* **1988**, *147*, 135.

- (12) One intriguing exception to this categorization is the neutral iron complex $[(\text{MeN}=\text{C}(\text{Ph})\text{C}(\text{Ph})=\text{O})\text{Fe}(\text{CO})_3]$, whose bond distances fall between the two groups in the histograms (shown in cyan in Figure 1). Consequently, a natural suggestion is that it is an Fe(I) complex coordinated by the monoanionic α -iminoketone π radical. However, the C–O stretching frequencies of the carbonyl ligands are akin to those reported for $[(\text{cyclopentadiene})\text{Fe}^0(\text{CO})_3]$ (see next reference) favoring an Fe(0) formulation and the absence of a ligand π radical.
- (13) Davison, A.; Green, M. L. H.; Wilkinson, G. *J. Chem. Soc.* **1961**, 3172.

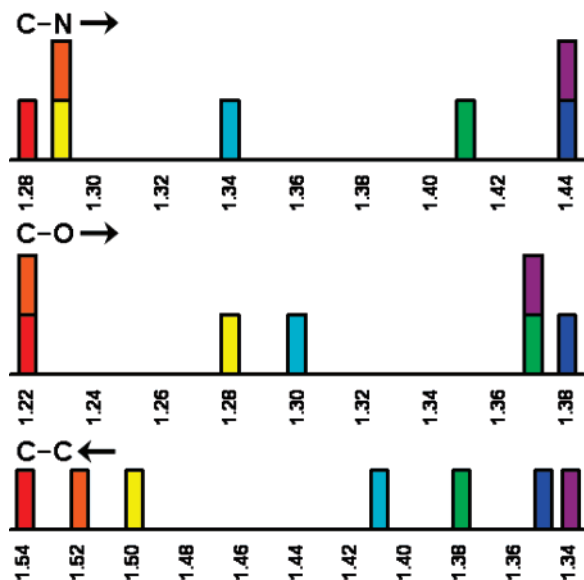
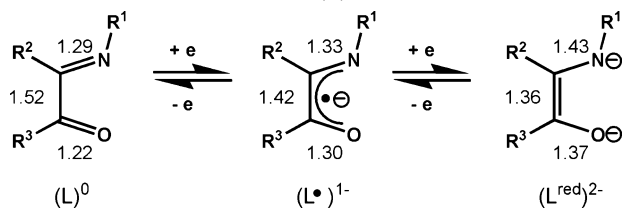


Figure 1. Histogram of the bond distances (Å) within the N–C–C–O backbone of structurally characterized transition-metal complexes containing a bidentate α -iminoketone ligand ($N^{\wedge}-O^{\wedge}$). Color key: $[(N^{\wedge}-O^{\wedge})Pd(\eta^2-1\text{-methoxycycloocten-5-yl})]^+$ is in red; $[(N^{\wedge}-O^{\wedge})Pd(\eta^2-5\text{-methoxycycloocten-6-yl})]^+$ is in orange; $[(N^{\wedge}-O^{\wedge})_2MnCl_2]$ is in yellow; $[(N^{\wedge}-O^{\wedge})Fe(CO)_3]$ is in cyan; $[(N^{\wedge}-O^{\wedge})Ti(OAr)_2]$ is in green; $[(N^{\wedge}-O^{\wedge})Zr(OAr)_2]$ is in dark blue; and $[(N^{\wedge}-O^{\wedge})Hf(\text{diamido-}N\text{-heterocyclic-carbene})]$ is in purple.

Scheme 1. Different Redox States for the α -Iminoketone Ligand with Their Characteristic Bond Distances (Å)



minated to dianionic enamidolates with a C=C double bond and C–N/C–O single bonds.

In principle, α -iminoketones exist in three different oxidation levels as follows: (a) the neutral α -iminoketone, (L^0); (b) the π -radical monoanion, ($L^{\bullet-}$); and (c) the closed-shell dianion, ($L^{\text{red}2-}$). Scheme 1 shows these different redox states along with their characteristic bond distances.¹⁵ The radical anion form of α -iminoketones ($L^{\bullet-}$) has been established by electron paramagnetic resonance (EPR) spectroscopy.^{16,17} However, structural characterization is still lacking. For the related α -diimine ligands, the monoanionic π -radical state has been described in detail for homoleptic transition-metal complexes featuring nickel^{18,19} cobalt,¹⁹ and

(14) The $[(N^{\wedge}-O^{\wedge})_2MnCl_2]$ complex contains a long C–O bond at 1.28 Å, which is an outlier. The C–N and C–C bond distances are in good agreement with a neutral ligand, which would imply a double C=O bond. One explanation for the unexpectedly long C–O bond is that the carbonyl is conjugated to a vinyl group, and thus, one of its tautomers formally contains a C–O single bond.

(15) The bond distances for the π -radical oxidation state of the ligand were taken from this work.

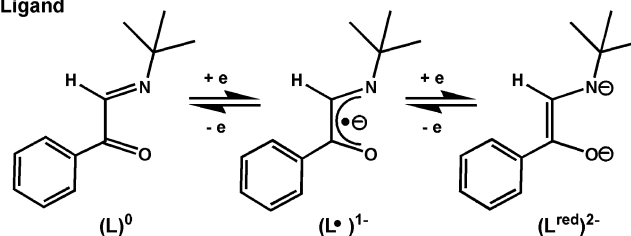
(16) Bessenbacher, C.; Kaim, W. Z. *Anorg. Allg. Chem.* **1989**, 577, 39.

(17) Alberti, A.; Camaggi, C. M. *J. Organomet. Chem.* **1979**, 181, 355.

(18) Muresan, N.; Chlopek, K.; Weyhermüller, T.; Neese, F.; Wieghardt, K. **2007**, 46, 5327.

(19) Khusniyarov, M. M.; Harms, K.; Burghaus, O.; Sundermeyer, J. *Eur. J. Inorg. Chem.* **2006**, 2985.

Chart 1
Ligand



Complexes

$[Ni^{II}(L^{\bullet})_2]$	(S = 0)	(1)
$[Ni^{II}(\text{trans-}(L)_2)(CH_3CN)_2](PF_6)_2$	(S = 1)	(2)
$[Co^{II}(L^{\bullet})_2]$	(S = 1/2)	(3)
$[Co^{II}(\text{trans-}(L)_2)(CH_3CN)_2](PF_6)_2$	(S = 3/2)	(4)

zinc centers.^{20,21} Thus, we set out to study this redox state of α -iminoketone ligands. In this paper, bis(α -iminoketone) complexes of nickel and cobalt are presented (Chart 1). We also report our interrogations into their electronic structures using spectroscopic methods and density functional theoretical (DFT) calculations.

II. Experimental Section

All syntheses were carried out using standard glovebox and Schlenk techniques in the absence of water and dioxygen, unless otherwise noted. Dry solvents were purchased from Fluka and used without further purification. Benzene- d_6 and CD_3CN were purchased from Cambridge Isotope Laboratories, Inc., degassed via repeated freeze–pump–thaw cycles, and dried over 3 Å molecular sieves. Sodium metal was purchased from Aldrich and washed with hexanes prior to use. The reagents $Ni(COD)_2$, $CoCl_2$, and $[Cp_2Fe](PF_6)$ were purchased from Strem and used without further purification (COD = 1,5-cyclooctadiene). The neutral α -iminoketone ligand ($t\text{-Bu}N=CH-C(\text{Ph})=O$) was prepared as described in the literature.^{22,23}

$[(L^{\bullet})_2Ni]$ (1). The neutral α -iminoketone ligand ($t\text{-Bu}N=CH-C(\text{Ph})=O$) (0.483 g, 2.55 mmol) was dissolved in n -pentane (5 mL). This solution was then added dropwise to a stirring suspension of $Ni(COD)_2$ (0.358 g, 1.28 mmol) in n -pentane (5 mL). After it was stirred for 24 h, the dark-purple solution was filtered to obtain a black-purple powder, which was washed with n -pentane. More powder was obtained by evaporating the filtrate under reduced pressure and washing the resultant residue with minimal CH_3CN . Single crystals of X-ray quality were grown from the CH_3CN filtrate at 22 °C. Yield: 0.502 g (90%). Anal. Calcd for $C_{24}H_{30}N_2NiO_2$: C, 65.93; H, 6.92; N, 6.41. Found: C, 65.54; H, 6.82; N, 6.30. ¹H NMR (400 MHz, C_6D_6 , 300 K): δ = 2.38 (9H, $t\text{-Bu}$), 6.32 (dd, 2H, J = 7.5 and 8.3 Hz, $m\text{-Ph}$), 9.32 (tt, 1H, J = 7.5 and 1.0 Hz, $p\text{-Ph}$), 9.52 (dd, 2H, J = 8.3 and 1.0 Hz, $o\text{-Ph}$), 9.99 (1H, NH). ¹³C NMR (100 MHz, C_6D_6 , 300 K): δ = 22.6, 75.2, 109.6, 114.4, 121.5, 139.6, 142.6, 171.4.

$[\text{trans-}(L)_2Ni(CH_3CN)_2](PF_6)_2$ (2). The complex $[(L^{\bullet})_2Ni]$ (72.0 mg, 0.165 mmol) was mixed with 2 equiv of $[Cp_2Fe](PF_6)$ (109 mg, 0.329 mmol) as solids. Acetonitrile (8 mL) was added, and

(20) Rijnberg, E.; Richter, B.; Thiele, K. H.; Boersma, J.; Veldman, N.; Spek, A. L.; van Koten, G. *Inorg. Chem.* **1998**, 37, 56.

(21) Gardiner, M. G.; Hanson, G. R.; Henderson, M. J.; Lee, F. C.; Raston, C. L. *Inorg. Chem.* **1994**, 33, 2456.

(22) Alcaide, B.; Escobar, G.; Pérez-Ossorio, R.; Plumet, J.; Sanz, D. *J. Chem. Res., Synop.* **1984**, 144.

(23) Alcaide, B.; Escobar, G.; Pérez-Ossorio, R.; Plumet, J.; Sanz, D. *J. Chem. Res., Miniprint* **1984**, 1466.

Table 1. Crystallographic Data for **1**, **2**·CH₃CN, **3**, and **4**·CH₃CN

	1	2 ·CH ₃ CN	3	4 ·CH ₃ CN
chemical formula	C ₂₄ H ₃₀ N ₂ NiO ₂	C ₃₀ H ₃₉ F ₁₂ N ₅ NiO ₂ P ₂	C ₂₄ H ₃₀ CoN ₂ O ₂	C ₃₀ H ₃₉ CoF ₁₂ N ₅ O ₂ P ₂
cryst size, mm ³	0.43 × 0.32 × 0.06	0.40 × 0.30 × 0.24	0.06 × 0.06 × 0.03	0.24 × 0.24 × 0.06
fw	437.21	850.31	437.43	850.53
space group	<i>Pbcn</i> , No. 60	<i>P2₁/c</i> , No. 14	<i>Pbcn</i> , No. 60	<i>P2₁/c</i> , No. 14
<i>a</i> , Å	10.2304(3)	11.237(3)	10.3003(5)	11.2058(2)
<i>b</i> , Å	11.0782(3)	15.009(4)	11.1678(5)	14.8769(3)
<i>c</i> , Å	18.7722(5)	22.035(6)	18.7003(7)	21.9353(5)
α, deg	90	90	90	90
β, deg	90	90.186(5)	90	90.300(3)
γ, deg	90	90	90	90
<i>V</i> , Å ³	2127.5(1)	3716.3(17)	2151.13(16)	3656.73(13)
<i>Z</i>	4	4	4	4
<i>T</i> , K	100(2)	100(2)	100(2)	100(2)
ρ calculated, g cm ⁻³	1.365	1.520	1.351	1.545
reflns collected/2Θ _{max}	73884/80.0	124485/ 70.0	39989/65.0	61550/55.0
unique reflns/ <i>I</i> > 2σ(<i>I</i>)	6587/5666	16332/14975	3895/3057	8390/6313
no. params/restraints	135/0	472/0	135/0	478/0
λ, Å/μ(Kα), cm ⁻¹	0.71073/9.34	0.71073/7.04	0.71073/8.20	0.71073/6.54
R1 ^a /GOF ^b	0.0350/1.084	0.0338/1.084	0.0372/1.061	0.0420/1.016
wR2 ^c (<i>I</i> > 2σ(<i>I</i>))	0.0784	0.0830	0.0805	0.0897
residual density/e Å ⁻³	+0.556/−0.466	+0.932/−0.733	+0.520/−0.404	+0.475/−0.353

^a Observation criterion: $I > 2\sigma(I)$. $R1 = \sum ||F_o| - |F_c|| / \sum |F_o|$. ^b GOF = $[\sum (w(F_o^2 - F_c^2)^2) / (n - p)]^{1/2}$. ^c wR2 = $[\sum (w(F_o^2 - F_c^2)^2) / \sum (w(F_o^2)^2)]^{1/2}$ where $w = 1/\sigma^2(F_o^2) + (aP)^2 + bP$, $P = (F_o^2 + 2F_c^2)/3$.

the solution rapidly changed color from dark purple to yellow. After it was stirred for 30 min, the solution was evaporated under reduced pressure. The resultant residue was washed liberally with THF, followed by extraction with CH₃CN and filtration through Celite. The solvent was removed completely under reduced pressure to give a pale-yellow powder. Single crystals of X-ray quality were grown from the vapor diffusion of Et₂O into a concentrated CH₃-CN solution of **2**. Yield: 115 mg (85%). Anal. Calcd for C₂₈H₃₆F₁₂N₄NiO₂P₂: C, 41.56; H, 4.48; N, 6.92. Found: C, 41.65; H, 4.50; N, 7.08. In CD₃CN solution, compound **2** is in equilibrium with a diamagnetic species, presumably square-planar [(L)₂Ni]²⁺ in ~3:2 ratio at 22 °C. ¹H NMR (400 MHz, CD₃CN, 300 K): δ = 5 (v. br.), 9.11, 9.45, 11.0, 11.1. For the diamagnetic species, δ = 1.30 (9H, *t*-Bu), 7.50 (t, 2H, *J* = 7.6 Hz, *m*-Ph), 7.63 (t, 1H, *J* = 7.5 Hz, *p*-Ph), 8.02 (1H, NH), 8.09 (d, 2H, *J* = 7.4 Hz, *o*-Ph).

[(L)₂Co] (**3**). The α-iminoketone ligand L (450 mg, 2.38 mmol), CoCl₂ (154 mg, 1.19 mmol), and Na metal (56.0 mg, 2.44 mmol) were added to a glass vessel. Dimethoxyether (DME, 15 mL) was added, and the reaction mixture was vigorously stirred for 16 h. The solvent was completely removed under reduced pressure. Pentane (2 mL) was added to the crude residue, which was then further dried under reduced pressure. The residue was extracted with C₆H₆, followed by filtration through Celite and evaporation of the solvent under reduced pressure. A dark-brown powder was thus obtained, and it was washed liberally with pentane. Single crystals of X-ray quality were grown from the vapor diffusion of pentane into a concentrated C₆H₆ solution of **3**. Yield: 250 mg (50%). Anal. Calcd for C₂₄H₃₀CoN₂O₂: C, 65.90; H, 6.91; N, 6.40. Found: C, 65.63; H, 6.79; N, 6.28. ¹H NMR (400 MHz, C₆D₆, 300 K): δ = −17.8, −7.4, 69.8, 74.7.

[*trans*-(L)₂Co(CH₃CN)₂](PF₆)₂ (**4**). The complex [(L)₂Co] (62.0 mg, 0.142 mmol) was mixed with 2 equiv of [Cp₂Fe](PF₆) (94.0 mg, 0.284 mmol) as solids. Acetonitrile (8 mL) was added, and the resultant solution rapidly changed color from dark brown to yellow. After it was stirred for 30 min, the solution was evaporated under reduced pressure. The resultant residue was washed liberally with THF, followed by extraction with CH₃CN and filtration through Celite. The solvent was removed completely under reduced pressure to give a yellow powder. Single orange-yellow crystals of X-ray quality were grown from the vapor diffusion of Et₂O into

a concentrated CH₃CN solution of **4**. Yield: 92.0 mg (80%). Anal. Calcd for C₂₈CoH₃₆F₁₂N₄O₂P₂: C, 41.55; H, 4.48; N, 6.92. Found: C, 41.42; H, 4.66; N, 7.12. ¹H NMR (400 MHz, CD₃CN, 300 K): δ = −35.4, 7.53, 8.06, 17.74, 18.48, 29.93.

X-ray Crystallographic Data Collection and Refinement of the Structures. A single dark-purple crystal of **1**, a yellow crystal of **2**, a dark-orange-brown crystal of **3**, and an orange crystal of **4** were coated with perfluoropolyether, picked up with nylon loops, and mounted in the nitrogen cold stream of the diffractometer. A Bruker-Nonius Kappa-CCD diffractometer equipped with a Mo-target rotating-anode X-ray source and a graphite monochromator (Mo Kα, λ = 0.71073 Å) was used. Final cell constants were obtained from least-squares fits of all measured reflections. The structures were readily solved by direct methods and subsequent difference Fourier techniques. The Siemens *SHELXTL*²⁴ software package was used for the solution and creation of the artwork of the structure, and *SHELXL97*²⁵ was used for the refinement. All non-hydrogen atoms were refined anisotropically. Hydrogen atoms were placed at calculated positions and refined as riding atoms with isotropic displacement parameters. Crystallographic data of the compounds are listed in Table 1.

Physical Measurements. Electronic spectra of complexes were recorded with a Perkin-Elmer double-beam photometer (300–2000 nm). Cyclic voltammograms were recorded with an EG&G potentiostat/galvanostat. Variable-field (0.01 or 1 T) and variable temperature (4–300 K) magnetization data were recorded on a SQUID magnetometer (MPMS Quantum Design). The experimental magnetic susceptibility data were corrected for underlying diamagnetism using tabulated Pascal's constants. X-band EPR spectra were recorded on a Bruker ESP 300 spectrometer and simulated with the *XSophe* program, which was written by Hanson et al.²⁶ and distributed by Bruker Biospin GmbH. NMR spectra were recorded on Varian Mercury 400 MHz instruments at ambient temperature.

(24) In *SHELXTL*, version 5; Siemens Analytical X-ray Instruments, Inc.: Madison, WI, 1994.

(25) Sheldrick, G. M. In *SHELXL97*; University of Göttingen: Göttingen, Germany, 1997.

(26) Hanson, G. R.; Gates, K. E.; Noble, C. J.; Griffin, M.; Mitchell, A.; Benson, S. J. *Inorg. Biochem.* **2004**, *98*, 903.

Calculations. All calculations were done with the ORCA program package.²⁷ The geometry optimizations were carried out at the B3LYP level^{28–30} of DFT. The all-electron Gaussian basis sets used were those reported by the Ahlrichs group.^{31,32} For nickel, cobalt, nitrogen, and oxygen atoms, the triple- ζ -quality basis sets with one set of polarization functions were used (TZVP).³¹ The carbon and hydrogen atoms were described by smaller polarized split-valence SV(P) basis sets (double- ζ -quality in the valence region with a polarizing set of d functions on the non-hydrogen atoms).³² The self-consistent field calculations were tightly converged ($1 \times 10^{-8} E_h$ in energy, $1 \times 10^{-7} E_h$ in the density change, and $1 \times 10^{-7} E_h$ in the maximum element of the DIIS error vector). The geometries were considered converged after the energy change was less than $5 \times 10^{-6} E_h$, the gradient norm and maximum gradient element were smaller than 1×10^{-4} and $3 \times 10^{-4} E_h/\text{bohr}$, respectively, and the root-mean-square and maximum displacements of the atoms were smaller than 2×10^{-3} and 4×10^{-3} bohr, respectively. The energies of the excited high-spin states were approximately calculated using geometries obtained from the broken-symmetry calculations with the appropriate total spin.

III. Results and Discussion

Syntheses and Characterization of Complexes. To install the α -iminoketone ligand (*t*-Bu)N=CH–C(Ph)=O (abbreviated as L), synthetic routes were employed that have been used by the groups of Holm,³³ tom Dieck,^{34–37} and Walther^{38,39} for preparing bis(α -diimine)metal complexes.

The neutral bis(ligand)nickel complex [(L*)₂Ni] (**1**) was obtained as a dark-black-purple powder in good yield (90%) from mixing Ni(COD)₂ with 2 equiv of ligand in *n*-pentane. Complex **1** is diamagnetic ($S = 0$) based on its NMR spectra. Notably, the ¹H NMR spectrum contains significantly deshielded peaks for the *p*-Ph (δ 9.32), *o*-Ph (δ 9.52), and iminoformyl (δ 9.99) protons (Supporting Information). A VT-NMR study of **1** from -60 to 60 °C revealed no changes in the ¹H NMR spectrum.

The cyclic voltammogram for **1** is shown in Figure 2. A quasi-reversible electron-transfer wave is observed at -0.84 V (200 mV/s, 0.1 M [N(*n*-Bu)₄](PF₆) in THF, vs Fc⁺/Fc). This feature corresponds to a two-electron oxidation based on the following experiments. The addition of 1 equiv of the oxidant [Cp₂Fe](PF₆) to **1** in CH₃CN resulted in a mixture of starting material and a new product, later identified as

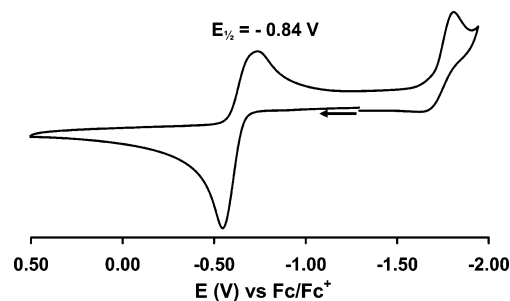


Figure 2. Cyclic voltammetry of **1** (0.1 M [N(*n*-Bu)₄](PF₆) in THF, 22 °C, glassy-carbon working electrode, 200 mV/s scan rate, and internal ferrocene (Fc) standard).

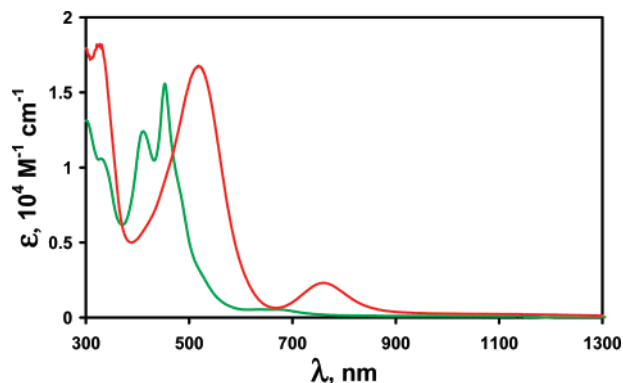


Figure 3. Electronic spectra of **1** (red) and **3** (green) in C₆H₆.

[*trans*-(L)₂Ni(CH₃CN)₂](PF₆)₂ (**2**) (by UV–vis and ¹H NMR spectroscopy). The addition of 2 equiv of [Cp₂Fe](PF₆) resulted in the clean conversion to **2**. Interestingly, a solution of **2** contains two distinct species, as elucidated by ¹H NMR spectroscopy. One of the species, identified by its solid-state structure as the solvento species [*trans*-(L)₂Ni(CH₃CN)₂]²⁺, is paramagnetic, which is characteristic of an octahedral Ni(II) $S = 1$ complex. The other one is diamagnetic, which is believed to arise from the square-planar Ni(II) complex without any coordinated solvent, [(L)₂Ni]²⁺.

The bis(ligand)cobalt complex [(L*)₂Co] (**3**) was synthesized by stirring 2 equiv of sodium metal, 2 equiv of ligand, and CoCl₂ in DME. Complex **3** is obtained in moderate yield (50%) as a dark-brown powder. Unlike **1**, no reversible features are observed in the cyclic voltammogram of **3**. An irreversible wave at -0.6 V is observed that may be analogous to the quasi-reversible wave measured for **1** (200 to 1000 mV/s, 0.1 M [N(*n*-Bu)₄](PF₆) in THF, vs Fc⁺/Fc). The cobalt complex **3** can also be oxidized by two electrons with 2 equiv of [Cp₂Fe](PF₆) in CH₃CN to provide the octahedral compound [*trans*-(L)₂Co(CH₃CN)₂](PF₆)₂ (**4**).

The electronic spectra for complexes **1** and **3** are shown in Figure 3, and the absorption maxima for **1–4** are listed in Table 2. Complexes **1** and **3** display intense absorption maxima from 300 to 600 nm ($\epsilon \sim 10^4 \text{ M}^{-1} \text{ cm}^{-1}$). Weaker absorptions for **1** and **3** are also observed at 760 ($\epsilon = 2000 \text{ M}^{-1} \text{ cm}^{-1}$) and 650 nm ($\epsilon = 500$), respectively. Notably absent are intense ligand-to-ligand charge-transfer (LLCT) bands in the region from 700 to 800 nm, which are characteristic of square-planar complexes with two π -radical

- (27) Neese, F. In *ORCA, an Ab Initio, Density Functional and Semiempirical Electronic Structure Program Package*, version 2.4, revision 36; Max-Planck-Institut für Bioanorganische Chemie: Mülheim/Ruhr, Germany, May, 2005.
- (28) Becke, A. D. *J. Chem. Phys.* **1993**, *98*, 5648.
- (29) Lee, C. T.; Yang, W. T.; Parr, R. G. *Phys. Review B: At., Mol., Opt. Phys.* **1988**, *37*, 785.
- (30) Becke, A. D. *J. Chem. Phys.* **1986**, *84*, 4524.
- (31) Schäfer, A.; Huber, C.; Ahlrichs, R. *J. Chem. Phys.* **1994**, *100*, 5829.
- (32) Schäfer, A.; Horn, H.; Ahlrichs, R. *J. Chem. Phys.* **1992**, *97*, 2571.
- (33) Balch, A. L.; Holm, R. H. *J. Am. Chem. Soc.* **1966**, *88*, 5201.
- (34) tom Dieck, H.; Svoboda, M.; Greiser, T. *Z. Naturforsch., B: Chem. Sci.* **1981**, *36*, 823.
- (35) tom Dieck, H.; Bruder, H. *J. Chem. Soc., Chem. Commun.* **1977**, 24.
- (36) tom Dieck, H.; Svoboda, M.; Kopf, J. *Z. Naturforsch., B: Chem. Sci.* **1978**, *33*, 1381.
- (37) tom Dieck, H.; Dietrich, J. *Angew. Chem., Int. Ed. Eng.* **1985**, *24*, 781.
- (38) Walther, D.; Kreisel, G.; Kirmse, R. *Z. Anorg. Allg. Chem.* **1982**, 487, 149.
- (39) Kirmse, R.; Stach, J.; Walther, D.; Bottcher, R. *Z. Chem.* **1980**, *20*, 224.

Table 2. Electronic Spectra of Complexes **1–4** at 22 °C

	λ_{max} , nm (ϵ , $10^3 \text{ M}^{-1} \text{ cm}^{-1}$)
1 ^a	320 (18), 520 (17), 760 (2.0)
2 ^b	255 (13), 310 sh
3 ^a	300 (13), 330 sh (11), 410 (12), 450 (15), 650 (0.5)
4 ^b	255 (13), 360 sh

^a In C₆H₆, ^b In CH₃CN.

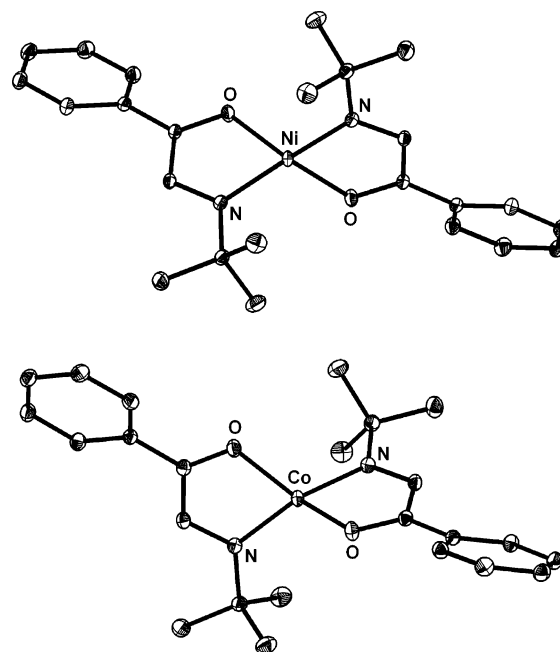
Table 3. Selected Angles (deg) and Bond Distances (Å) for **1–4**

	1	2 ·CH ₃ CN	3	4 ·CH ₃ CN
dihedral angle	83.8	0.9	86.5	1.3
O–M–N _{imine}	82.99(3)	78.57(3) 78.79(3)	83.97(4)	76.98(7) 77.09(7)
M–O	1.9342(6)	2.0587(8) 2.0663(8)	1.955(1)	2.080(2) 2.083(2)
M–N _{imine}	1.9210(7)	2.1113(8) 2.1139(8)	1.954(1)	2.138(2) 2.141(2)
M–N _{solvent}		2.0472(9) 2.0518(9)		2.090(2) 2.084(2)
O–C _{ketone}	1.2900(9)	1.238(1) 1.237(1)	1.302(2)	1.231(3) 1.228(3)
C _{ketone} –C _{imine}	1.415(1)	1.501(1) 1.500(1)	1.415(2)	1.487(3) 1.497(3)
C _{imine} –N _{imine}	1.3210(9)	1.276(1) 1.274(1)	1.326(2)	1.263(3) 1.264(3)

ligands.^{40–43} Therefore, the lack of intense LLCT bands for **1** and **3** suggests nonplanar geometries, which were confirmed by X-ray crystallography (vide infra). The electronic spectra for **2** and **4** are nearly identical with intense bands at 255 nm ($\epsilon = 13\,000 \text{ M}^{-1} \text{ cm}^{-1}$) and the absence of any significant absorptions from 400 to 2000 nm (Supporting Information). The latter is consistent with complexes that do not contain any ligand π -radical character.

Solid-State Structures. The molecular structures for **1–4** have been determined at 100 K by single-crystal X-ray diffraction studies. Crystallographic details are provided in Table 1, and important bond parameters are presented in Table 3.

Figure 4 shows the solid-state structures of **1** and **3**. They appear isostructural with a metal center in tetrahedral geometry. The dihedral angle (the angle between the two five-membered metal–ligand rings) for **1** is 83.8° and 86.5° for **3**. The tetrahedral geometry was unexpected for the neutral nickel and cobalt complexes because there are many examples of four-coordinate metal complexes with two *o*-iminobenzosemiquinonate π -radical ligands, which are typically square planar.^{44–49} A few exceptions exist with dihedral angles ranging from 32.0° to 72.0°.^{50–52} However,

**Figure 4.** Structure of the neutral molecules in crystals of **1** (top) and **3** (bottom).

these exceptional dihedral angles are attributed to steric repulsion between the two ligands or to the presence of an additional weak donor. The α -iminoketone ligand used here is relatively unhindered, so a planar arrangement is possible from pure steric considerations. The observed tetrahedral geometry may indicate a slight electronic preference over the square-planar arrangement (vide infra).

A closer inspection of the bond parameters in **1** and **3** reveals unusual bond distances within the ligand backbone (O–C–C–N). Compared with other structurally characterized α -iminoketone complexes (including **2** and **4**),⁵³ the C–O and C–N bond distances are significantly elongated while the C–C bond distances are much shorter, indicating the presence of two π -radical ligands ($L^{\bullet-}$).

Figure 5 shows the solid-state structures of the dicationic **2** and **4**. Both complexes are octahedral with two trans-coordinated acetonitriles. The α -iminoketone ligands occupy the equatorial plane with a nearly zero dihedral angle between them. The bond distances in the ligand backbones are quite similar between the two structures. The average C–O ($1.233 \pm 0.005 \text{ \AA}$), C–C ($1.496 \pm 0.009 \text{ \AA}$), and C–N ($1.269 \pm 0.007 \text{ \AA}$) bond distances are consistent with a C–C single bond and C=O/C=N double bonds. Thus for **1** and **3**, the

(40) Blanchard, S.; Neese, F.; Bothe, E.; Bill, E.; Weyhermüller, T.; Wieghardt, K. *Inorg. Chem.* **2005**, *44*, 3636.

(41) Chlopek, K.; Bothe, E.; Neese, F.; Weyhermüller, T.; Wieghardt, K. *Inorg. Chem.* **2006**, *45*, 6298.

(42) Herebian, D.; Wieghardt, K. E.; Neese, F. *J. Am. Chem. Soc.* **2003**, *125*, 10997.

(43) Herebian, D.; Bothe, E.; Neese, F.; Weyhermüller, T.; Wieghardt, K. *J. Am. Chem. Soc.* **2003**, *125*, 9116.

(44) Abakumov, G. A.; Poddel'sky, A. I.; Bubnov, M. P.; Fukin, G. K.; Abakumova, L. G.; Iksorskii, V. N.; Cherkasov, V. K. *Inorg. Chim. Acta* **2005**, *358*, 3829.

(45) Kokatam, S.; Weyhermüller, T.; Bothe, E.; Chaudhuri, P.; Wieghardt, K. *Inorg. Chem.* **2005**, *44*, 3709.

(46) Bill, E.; Bothe, E.; Chaudhuri, P.; Chlopek, K.; Herebian, D.; Kokatam, S.; Ray, K.; Weyhermüller, T.; Neese, F.; Wieghardt, K. *Chem.—Eur. J.* **2004**, *11*, 204.

(47) Poddel'sky, A. I.; Cherkasov, V. K.; Fukin, G. K.; Bubnov, M. P.; Abakumova, L. G.; Abakumov, G. A. *Inorg. Chim. Acta* **2004**, *357*, 3632.

(48) Sun, X. R.; Chun, H.; Hildenbrand, K.; Bothe, E.; Weyhermüller, T.; Neese, F.; Wieghardt, K. *Inorg. Chem.* **2002**, *41*, 4295.

(49) Chaudhuri, P.; Verani, C. N.; Bill, E.; Bothe, E.; Weyhermüller, T.; Wieghardt, K. *J. Am. Chem. Soc.* **2001**, *123*, 2213.

(50) Ye, S. F.; Sarkar, B.; Lissner, F.; Schleid, T.; van Slageren, J.; Fiedler, J.; Kaim, W. *Angew. Chem., Int. Ed.* **2005**, *44*, 2103.

(51) Speier, G.; Whalen, A. M.; Csihony, J.; Pierpont, C. G. *Inorg. Chem.* **1995**, *34*, 1355.

(52) Whalen, A. M.; Bhattacharya, S.; Pierpont, C. G. *Inorg. Chem.* **1994**, *33*, 347.

(53) We have excluded those complexes with amidolate ligands. One exception is again the neutral iron complex $\text{LFe}(\text{CO})_3$.

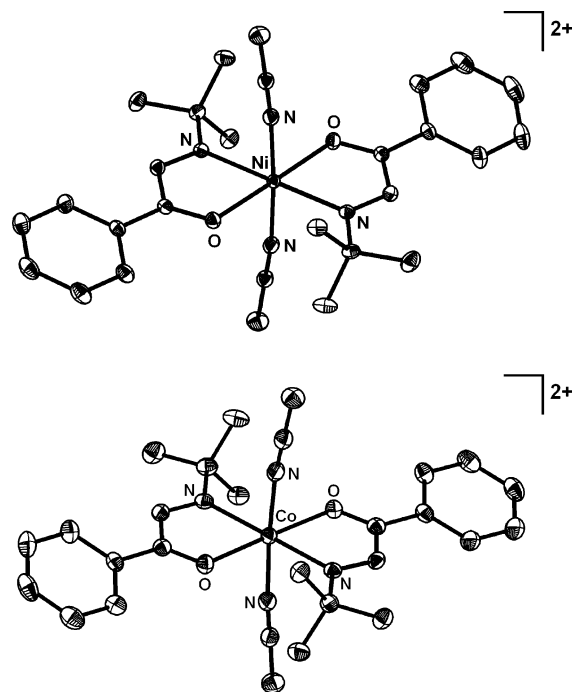


Figure 5. Structure of the dications in crystals of **2** (top) and **4** (bottom). Hydrogen atoms, PF_6^- counteranions, and solvent molecules have been omitted.

average C–O ($1.296 \pm 0.006 \text{ \AA}$), C–C ($1.415 \pm 0.001 \text{ \AA}$), and C–N ($1.324 \pm 0.003 \text{ \AA}$) bond distances are approximately half a bond order different from those observed in **2** and **4**. These bond parameters indicate that the α -iminoketone ligands in **1** and **3** are reduced to the monoanionic ligand π -radical form (L^\bullet) $^-$.

Magnetic Susceptibilities and EPR Spectroscopy. The expected $S = 1$ ground state of the octahedral Ni(II) dication in **2** was confirmed by magnetic susceptibility measurements on a solid sample of **2** (1.0 T, 4–300 K). The magnetic moment, μ_{eff} , is temperature-independent in the range of 10–300 K at $3.09 \mu_{\text{B}}$ (Supporting Information). The octahedral Co(II) dication in **4** is expected to have a $S = 3/2$ ground state, which was confirmed by an axial signal with a zero-field crossing at $g_{\text{eff}} \sim 4$ in its EPR spectrum at 4 K in frozen acetonitrile (Supporting Information).⁵⁴

Of the complexes reported here, **3** is perhaps the most interesting and convenient to study spectroscopically due to the presence of two ligand radicals in a complex with a $S = 1/2$ ground state (vide infra). The temperature-dependent plot of its effective magnetic moment is shown in Figure 6 (0.01 T, 4–300 K). The μ_{eff} value of **3** is constant in the range of 60–300 K at $2.36 \mu_{\text{B}}$, which is slightly above the spin-only value of $1.73 \mu_{\text{B}}$ for a $S = 1/2$ system. This data is consistent with a strong intramolecular antiferromagnetic coupling between two ligand radicals with $S = 1/2$ and a high-spin Co(II) center with $S = 3/2$. Assuming an energetically well-isolated magnetic ground state with total spin $S_{\text{tot}} = 1/2$, the plot was well simulated by adopting a remarkably large isotropic g value, $g_{\text{tot}} = 2.73$. Tetrahedral Co(II) centers are

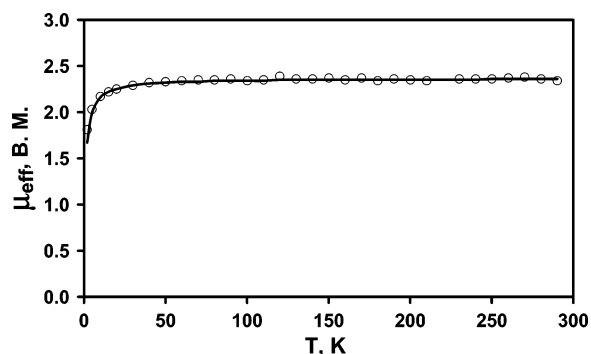


Figure 6. Temperature dependence of the magnetic moment, μ_{eff} , of **3** (shown in open circles, 0.01 T, 4–300 K). The solid line represents a spin-Hamiltonian simulation with total spin $S_{\text{tot}} = 1/2$ and an isotropic g value of 2.73. The experimental data was corrected for temperature-independent paramagnetism, χ_{TIP} , of $400 \times 10^{-6} \text{ cm}^3 \text{ mol}^{-1}$. Intermolecular coupling was considered by introducing a Weiss constant, θ , of -2 K to account for the low-temperature drop of μ_{eff} .

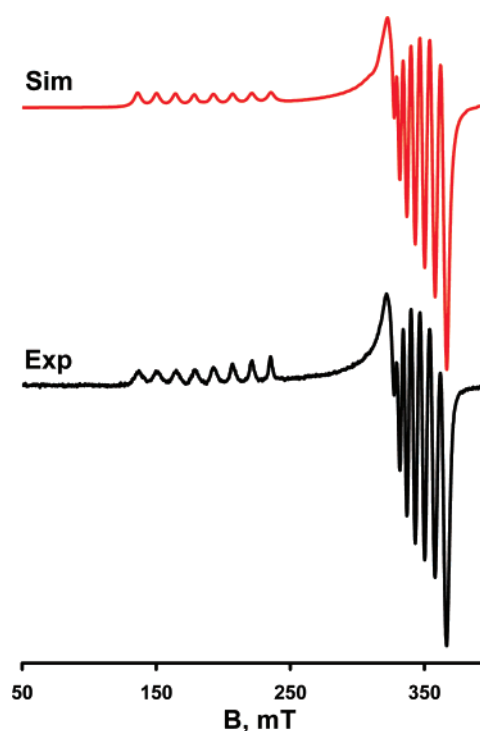


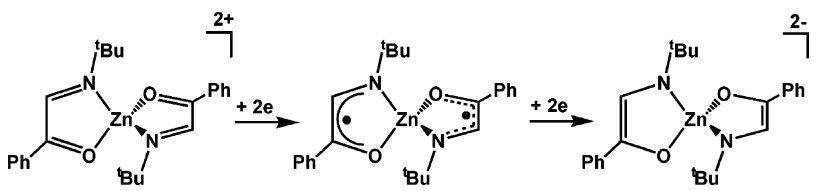
Figure 7. X-band EPR spectrum of **3** in toluene glass ($1 \times 10^{-3} \text{ M}$, 10.25 K, frequency = 9.44 GHz, modulation = 2 mT/100 kHz, power = 252 μW). See text for simulation parameters.

expected to have g values that deviate significantly from g_{e} due to spin–orbit coupling.⁵⁵ Moreover, the large calculated g value of 2.73 is reasonably close to the average g value of 2.62 derived from its EPR spectrum (vide infra).

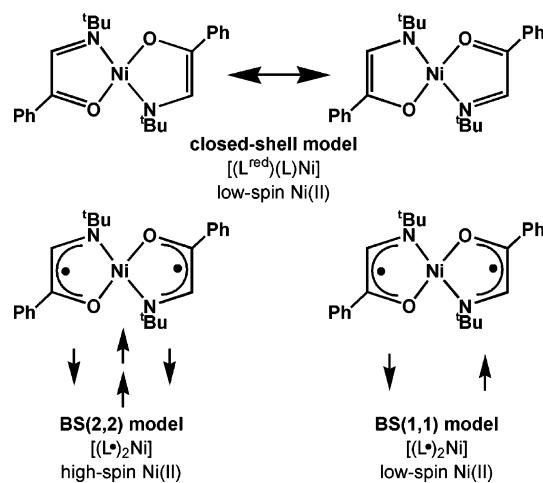
The X-band EPR spectrum of **3** in a frozen toluene glass at 10.25 K confirms the expected $S_{\text{tot}} = 1/2$ ground state (Figure 7). The spectrum shows a huge axial splitting with the following g values: $g_1 = 1.949$, $g_2 = 1.936$, and $g_3 = 3.620$ ($g_{\text{ave}} = 2.624$, where $g_{\text{ave}} = ((g_1^2 + g_2^2 + g_3^2)/3)^{1/2}$). Hyperfine coupling to the cobalt center ($I = 7/2$) is evident for all three g signals with magnetic hyperfine coupling

(54) Banci, L.; Bencini, A.; Benelli, C.; Gatteschi, D.; Zanchini, C. In *Struct and Bonding*; Springer-Verlag: Berlin, 1982; Vol. 52, p 38.

(55) Girerd, J.-J.; Journaux, Y. In *Physical Methods in Bioinorganic Chemistry: Spectroscopy and Magnetism*; Que, L., Jr., Ed.; University Science Books: Sausalito, CA, 2000; p 321.

Table 4. Selected Angles (deg) and Bond Distances (Å) for Calculated Bis(ligand)zinc Complexes


	$[(L^0)_2Zn]^{2+}$	$[(L^•)_2Zn]^0$	$[(L^{2-})_2Zn]^{2-}$
dihedral angle	78.5	77.5	78.3
O–Zn–N _{imine}	81.18	83.45	84.14
Zn–O	2.017	2.000	2.003
Zn–N _{imine}	2.068	2.038	2.055
O–C _{ketone}	1.260	1.300	1.350
C _{ketone} –C _{imine}	1.513	1.432	1.395
C _{imine} –N _{imine}	1.277	1.322	1.358

Scheme 2. DFT Models of Three Different Electronic Structures for **1**^a

^a The unpaired electrons are shown as localized on the ligand and/or nickel.

constants of $A = (50.00, 52.15, 240.0) \times 10^{-4} \text{ cm}^{-1}$ (with anisotropic line widths $\Gamma = (24.94, 22.76, 32.00) \times 10^{-4} \text{ cm}^{-1}$).

To isolate the metal contribution in the EPR values above, the total spin vector ($S_{\text{tot}} = 1/2$) can be split into two spin components, \hat{S}_{Co} and \hat{S}_{L} , where $S_{\text{Co}} = 3/2$ and \hat{S}_{L} is the combined spin vector of the two ligand radicals with $S_{\text{L}} = 1$ (vide infra). Projecting these spin components leads to the following relationships:⁵⁶

$$g_{\text{tot}} = \frac{5}{3}(g_{\text{Co}}) - \frac{2}{3}(g_{\text{Lig}}) \quad (1)$$

$$A_{\text{tot}} = \frac{5}{3}(A_{\text{Co}}) \quad (2)$$

With the use of eqs 1 and 2, the local g values and magnetic hyperfine coupling constants are obtained with respect to \hat{S}_{Co} : $g(\text{Co}) = 1.969, 1.962, 2.972$ (where $g_{\text{ave}}(\text{Co}) = 2.349$); and $A(\text{Co}) = (30.00, 31.29, 144.0) \times 10^{-4} \text{ cm}^{-1}$. The high g values and large coupling constants support the notion that the unpaired electron is localized on the metal,

(56) Bencini, A.; Gatteschi, D. *Electron Paramagnetic Resonance of Exchange-Coupled Systems*; Springer: Berlin, 1990.

Table 5. Selected Angles (deg) and Bond Distances (Å) for **1** and Its Optimized DFT-Calculated Models

	1	BS(2,2)	BS(1,1)	no BS
calcd energy ^a		0	+2.15	+2.17
dihedral angle	83.8	63.75	0.16	0.12
O–M–N _{imine}	82.99(3)	81.9	84.3	84.4
M–O	1.9342(6)	1.972	1.866	1.846
M–N _{imine}	1.9210(7)	2.002	1.949	1.920
O–C _{ketone}	1.2900(9)	1.294	1.310	1.308
C _{ketone} –C _{imine}	1.415(1)	1.432	1.412	1.409
C _{imine} –N _{imine}	1.3210(9)	1.320	1.327	1.332

^a Relative energies (kcal/mol).

as is the expected net result of a Co(II) high-spin center with three unpaired electrons coupled strongly to two ligand radicals.

DFT Calculations. In conjunction with the experimental studies, DFT calculations were conducted at the B3LYP level to garner a more complete bonding picture. First, the various redox states of the α -iminoketone ligand were explored by using model bis(ligand)zinc complexes $[(L^x)_2Zn]^n$ ($n = -2, 0, +2$). Then, the neutral $[(L^•)_2Ni]$ and $[(L^•)_2Co]$ complexes were calculated to better understand their electronic structures.

Zinc Reference Compounds. The model species $[(L^x)_2Zn]^n$ (for $n = -2, 0, +2$) were chosen because zinc(II) centers (d^{10} , $S_{\text{Zn}} = 0$) are relatively redox inert, and thus, any changes in the overall charge of the molecule should be reflected in the ligand oxidation level. Thus, two neutral ligands (L^0) for the $n = +2$ case, two π -radical ligands ($L^•$)[−] for $n = 0$, and two dianionic ligands ($L^{\text{red}})^{2-}$ for $n = -2$ are expected to be present. For all values of n , both the square-planar and the tetrahedral complexes were calculated using the B3LYP functional and spin-unrestricted methods. In all cases, the tetrahedral geometry was favored by 7–8 kcal/mol. Because of this clear trend, only the tetrahedral calculations are presented. For the calculated dication ($S = 0$), the bond distances are consistent with neutral α -iminoketone ligands, whereas the dianion ($S = 0$) features two enamidolate ligands with a C=C double bond and C–O/C–N single bonds (Table 4). Thus, the proper formulations for the theoretical dicationic and dianionic bis(ligand)zinc species are $[(L)_2Zn]^{2+}$ and $[(L^{\text{red}})_2Zn]^{2-}$, respectively.

The neutral tetrahedral bis(ligand)zinc species was modeled by using the broken-symmetry approach (vide infra).

Two scenarios were considered: a triplet ground state wherein the ligand π -radical electrons are parallel and a singlet ground state wherein these electrons are paired via a superexchange mechanism^{42,43} through the metal center. Only a small difference of 0.05 kcal/mol was found between the energies of the singlet and triplet states. Thus, there is essentially no preference between these two states; they are degenerate. Even the bond distances and angles in the calculated singlet and triplet structures are all identical. Notably, the bond distances in the ligand backbone are about halfway between those calculated for the $[(L)_2Zn]^{2+}$ and $[(L^{\text{red}})_2Zn]^{2-}$ models. Hence, the calculated bond distances for the neutral species are consistent with each ligand being reduced by one electron. Interestingly, these bond distances are remarkably similar to those observed in complexes **1** and **3**. This lends further evidence that the neutral bis(ligand)-metal compounds are best formulated as $[(L^{\bullet})_2M]^0$, featuring two ligand radicals and a divalent metal center.

$[(L^{\bullet})_2Ni]$ Calculations. Three models were considered for the $S = 0$ bis(ligand)nickel complex **1** (Scheme 2). One possibility invokes a low-spin Ni(II) center ($S_{Ni} = 0$) coordinated to $(L^{\text{red}})^{2-}$ and $(L)^0$. For this description, a closed-shell calculation is sufficient. Another hypothesis is a high-spin Ni(II) center ($S_{Ni} = 1$) that couples antiferromagnetically to two ligand π -radicals. The third model involves a low-spin Ni(II) center ($S_{Ni} = 0$) and two ligand radicals that couple to one another via the metal d orbitals. For the latter two, open-shell calculations are required with broken-symmetry techniques. For instance, the label BS(x,y) refers to a broken-symmetry state with x spin-up electrons and y spin-down electrons. The x and y electrons can be localized on different parts of the molecule, i.e., metal versus ligand, so that they are not forcibly paired. However, their spins can couple. The model with the $S_{Ni} = 1$ Ni(II) center with two ligand radicals can be described as BS(2,2), while BS(1,1) represents the $S_{Ni} = 0$ Ni(II) center with two ligand radicals.

All three calculations used the same input geometry, which was derived from the solid-state structure of **1**, and converged successfully. The structural parameters for the calculated models are given in Table 5. All models reproduce reasonably the bond distances in the ligand backbone (within 0.02 Å of the experimental data). This is not surprising, because all models *essentially* localize one electron on each ligand. While clearly the case for the open-shell cases, the “one-electron reduction per ligand” case may not be obvious in the closed-shell calculation. Recall that in the closed-shell model, one ligand is doubly reduced while the other ligand remains neutral. The charges on the two ligands are exchanged by resonance, so that *on average* each ligand is reduced by one electron.

Of the three, the BS(2,2) model is the lowest in energy by only 2 kcal/mol. The most striking difference is the prediction of the dihedral angles. The BS(2,2) structure is distorted tetrahedral with a dihedral angle of 63.75° (experimental 83.8°), whereas the other two models gave square-planar structures. We should stress that a four-coordinate Ni(II) center with $S_{Ni} = 0$ can only exist in a square-planar

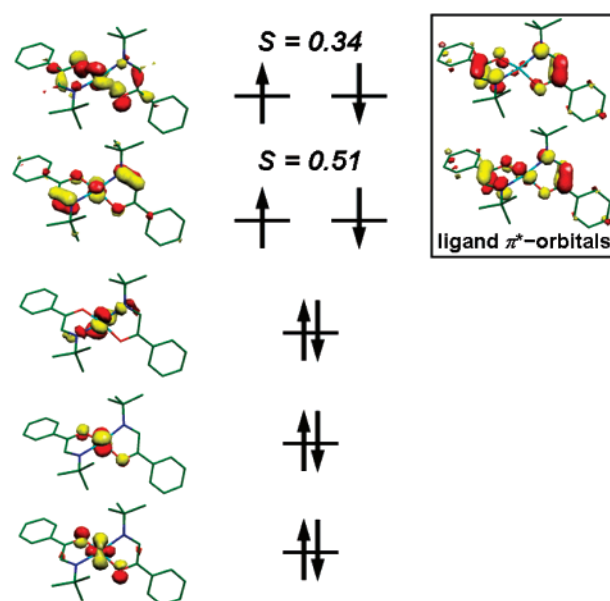


Figure 8. Qualitative MO diagram of the magnetic orbitals derived from BS(2,2) calculation of $[(L^{\bullet})_2Ni]$. The spatial overlap (S) of corresponding alpha and beta orbitals is given. If unspecified, $S = 1$.

arrangement. The preference for square-planar geometries in the closed-shell and BS(1,1) models can be further rationalized. In the BS(1,1) case, the two ligand π^* orbitals couple through d orbitals at nickel. However, in a tetrahedral geometry, the π^* orbitals would interact with d orbitals that are orthogonal, and thus, long-range ligand–ligand coupling is impossible.^{19,50} A similar argument applies for the closed-shell system, where a requirement for resonance would be at least one molecular orbital (MO) that encompasses π^* orbitals of both ligands.

Overall, the BS(2,2) model best matches the experimental data. The MO scheme (Figure 8) reveals three doubly occupied Ni d orbitals and two metal-based singly occupied molecular orbitals (SOMOs) in the spin-up manifold. The latter are coupled to two SOMOs, which are primarily the lowest unoccupied molecular orbital π^* orbitals of the neutral ligand, in the spin-down manifold with overlaps of 0.51 and 0.34. The MO diagram reflects the high-spin Ni(II) center ($S_{Ni} = 1$) that is antiferromagnetically coupled to two ligand π -system radicals ($S_{Lig1} = S_{Lig2} = 1/2$). The strength of this coupling can be calculated with Yamaguchi’s equation⁵⁷

$$J = -\frac{E_{HS} - E_{BS}}{\langle S^2 \rangle_{HS} - \langle S^2 \rangle_{BS}} \quad (3)$$

which approximates the spin–spin coupling constant (J) in a two-spin system described by the Hamiltonian, $\hat{H} = -2J\hat{S}_A \cdot \hat{S}_B$. The coupling constant is based on the energies (E) and spin-expectation values ($\langle S^2 \rangle$) of the broken symmetry and the high-spin states. For $[(L^{\bullet})_2Ni]$, the three-spin Hamiltonian can be written as $\hat{H} = -2J_1 \cdot \hat{S}_{Ni} \cdot \hat{S}_{Lig1} - 2J_2 \cdot \hat{S}_{Ni} \cdot \hat{S}_{Lig2} + 2J_3 \cdot \hat{S}_{Lig1} \cdot \hat{S}_{Lig2}$. Assuming that the $J_1 = J_2$ and supposing that the

(57) Soda, T.; Kitagawa, Y.; Onishi, T.; Takano, Y.; Shigeta, Y.; Nagao, H.; Yoshioka, Y.; Yamaguchi, K. *Chem. Phys. Lett.* **2000**, *319*, 223.

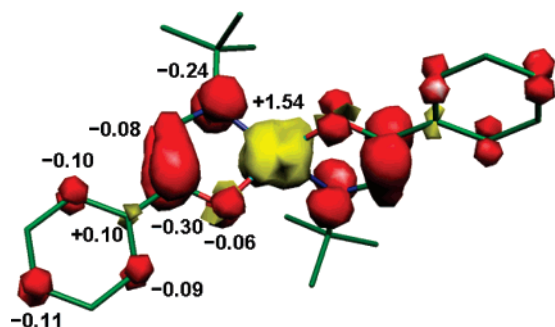


Figure 9. Spin-density plot shown with values as derived from the BS-(2,2) calculation for $[(L^*)_2Ni]$ (based on Mulliken spin population analysis).

ligand–ligand coupling is negligible relative to that of nickel–ligand coupling, the Hamiltonian is simplified to $-2J\hat{S}_{Ni} \cdot (\hat{S}_{Lig1} + \hat{S}_{Lig2})$. Furthermore, the two ligand spin vectors can be combined into one total ligand spin vector \hat{S}_L (where $S_L = 1$) since they are effectively ferromagnetically coupled due to their strong antiferromagnetic interaction with the nickel center (which is reflected in the observed singlet ground state up to 60 °C). With the Hamiltonian thus reduced to $-2J\hat{S}_{Ni} \cdot \hat{S}_L$, Yamaguchi's equation can be applied, and a value for J of -780 cm^{-1} is obtained.⁴⁰

A spin-density plot (Figure 9) further reinforces the picture of a high-spin Ni(II) center antiferromagnetically coupled to two ligand radicals by showing nearly two unpaired electrons at nickel and an opposite spin on each ligand that is approximately equivalent to one unpaired electron. Interestingly, some spin density delocalizes into the phenyl ring at the ortho and para carbons (about -0.10 per carbon). Recall that the protons attached to these carbons and the iminoformyl proton are all significantly deshielded in the 1H NMR spectrum of **1**. On the basis of the spin-density plot, one can suggest that the ligand radical delocalizes significantly into the phenyl ring ($\sim 20\%$). However, we note that the calculation predicts a coplanar arrangement of the phenyl ring and the metal–ligand plane, which maximizes this delocalization effect. In actuality, the ring is likely rotating rapidly.

$[(L^*)_2Co]$ Calculations. For the bis(ligand)cobalt complex ($S = 1/2$), we can envision three possible electronic structures: (1) a closed-shell molecule with a low-spin Co(II) center ($S_{Co} = 1/2$), one dianionic ligand, and one neutral ligand; (2) a BS(3,2) model featuring a high-spin Co(II) ($S_{Co} = 3/2$) coupled antiferromagnetically to two ligand radicals; or, (3) a BS(1,2) model featuring a low-spin Co(II) ($S_{Co} = 1/2$) with two ligand radicals coupled antiferromagnetically to one another. From what we learned with nickel, only the BS(3,2) formulation would give rise to the observed tetrahedral geometry. Figure 10 shows the optimized geometry of the BS(3,2) model along with some key structural parameters. The optimized structure agrees well with the experimental data, especially regarding the bond distances in the ligand backbone. The MO scheme (Figure 11) reveals two doubly occupied d orbitals, two ligand-based SOMOs that are coupled to two metal-based SOMOs, and one unpaired electron in the highest occupied SOMO, which is heavily localized on cobalt (86% d character). Akin to the

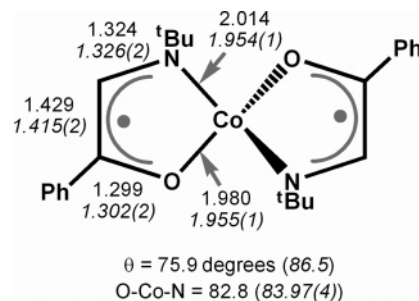


Figure 10. Selected angles (deg) and bond distances (Å) for the DFT-optimized BS(3,2) calculation of $[(L^*)_2Co]$. Experimental values are shown in italics.

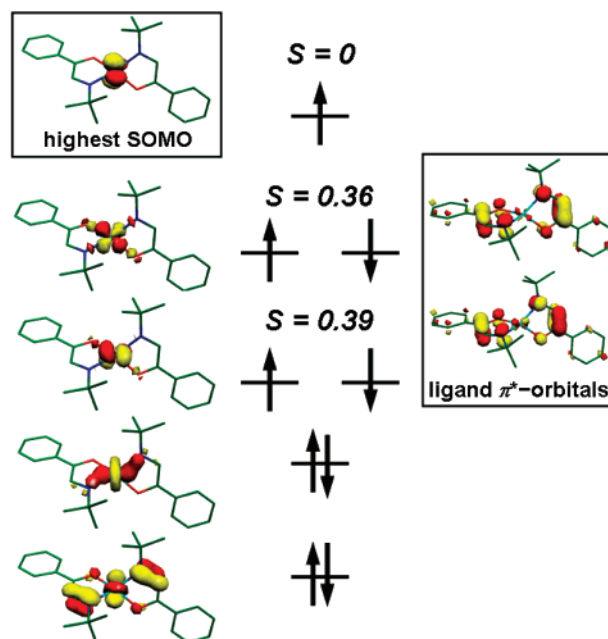


Figure 11. Qualitative MO diagram of the magnetic orbitals derived from BS(3,2) calculation of $[(L^*)_2Co]$. The spatial overlap (S) of corresponding alpha and beta orbitals is given. If unspecified, $S = 1$.

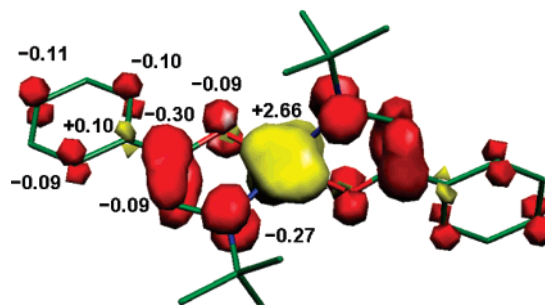


Figure 12. Spin-density plot shown with values as derived from the BS-(3,2) calculation of $[(L^*)_2Co]$ (based on Mulliken spin population analysis).

nickel case, the antiferromagnetic coupling constant between the two unpaired electrons on the metal and the two ligand-based π radicals can be estimated using Yamaguchi's equation. A coupling constant J of -504 cm^{-1} is calculated. In addition, the large metal character of the highest occupied SOMO is in agreement with the highly anisotropic EPR signal that was obtained experimentally. The spin-density plot (Figure 12) shows unpaired spins on both the metal and ligands that are consistent with high-spin Co(II) with three unpaired electrons and one electron per ligand, respectively.

IV. Summary

We have shown that the radical form (L^*)⁻ of the α -iminoketone ligand (*t*-Bu)N=CH-C(Ph)=O is a viable redox state. The bis(ligand)metal complexes of nickel and cobalt have been characterized by physical methods as well as theoretical calculations. A general electronic description for these complexes is that of a high-spin divalent metal center that is strongly coupled antiferromagnetically to two ligand radicals. In our DFT calculations, we have observed that even closed-shell electronic descriptions can predict ligand-backbone bond distances that are consistent with a ligand π radical. Thus, the assignment of ligand oxidation states based only on bond distances from solid-state structures can be misleading. Understanding the redox states of the

ligand and the metal center truly requires the use of several spectroscopic tools.

Acknowledgment. The authors thank Dr. Nicoleta Muresan and Prof. Dr. Frank Neese (University of Bonn) for helpful discussions. Heike Schucht, Andreas Göbels, Frank Reikowski, and Petra Höfer are acknowledged for technical assistance. C.C.L. is funded by the Alexander von Humboldt Foundation.

Supporting Information Available: Additional spectroscopic data, including ¹H NMR spectrum of **1**, electronic spectra of **2** and **4**, μ_{eff} vs *T* plot for **2**, and EPR spectrum of **4**. This material is available free of charge via the Internet at <http://pubs.acs.org>.

IC7008094